The GTeV Forward Spectrometer Acceptance Studies *

M. Albrow, A.I. Drozhdin, N.V, Mokhov
Fermi National Accelerator Laboratory
P.O. Box 500, Batavia, Illinois 60510

June 29, 2004

1 Introduction

The idea of running the CDF (or DØ) forward detectors in parallel with BTeV detector is discussed. The detector (called here GTeV detector) consists of quadrupole Roman Pot units placed in the BØ straight section and dipole Roman Pot units located near and far from the IP. Each quadrupole unit consists of four square $2 \times 2cm^2$ detectors placed from the closed orbit in the horizontal (X) and vertical (Y) plane. The dipole unit consists of three detectors placed in the top, bottom and only inside from the closed orbit. The detectors are made of a silicon wafer, about $400\mu m$ thick, on which is deposited a thin layer (say $50\mu m$) of diamond. The Roman pot positions are adjustable in the X or Y directions and can be moved according to the beam halo conditions in the Tevatron.

2 The GTeV Forward Spectrometer

The GTeV Forward Spectrometer detectors (Roman Pots) are placed downstream of the BØ quadrupole triplet and behind the first two and farther dipole magnets in the Tevatron lattice at the proton and antiproton side from the IP. This requires to replace several regular dipoles by the new stronger dipoles to provide space for the spectrometers. Tevatron Run-II lattice and lattice with two increased strength magnets instead of three normal strength magnets in the Tevatron B11 section is shown in Fig. 1. Magnetic field in two magnets is increased to 6.7 T compared to the normal field of 4.42 T. This provides space of about 4.0 m for Roman pots and 1.4 m for cryogenic bypass.

Horizontal and vertical β functions and horizontal dispersion in the Tevatron Run-II lattice and lattice with increased strength of magnets in the Tevatron A44, B11 and B15 sections are shown in Fig. 2. There is no visible difference in β and dispersion functions. Because of this we believe that there should not be a problem with beam stability in the new lattice.

Position of the detectors with respect to the IP and aperture of accelerator in this region are shown in Fig. 3. The dipole detectors are located at the distance of ~ 55 m and ~ 165 m from BØ. Roman Pots are located at $10\sigma_{y,x}$ from the center of the proton and antiproton beams (Fig. 4 and Tab. 1).

*Work supported by the Universities Research Association, Inc., under contract DE-AC02-76CH00300 with the U. S. Department of Energy.

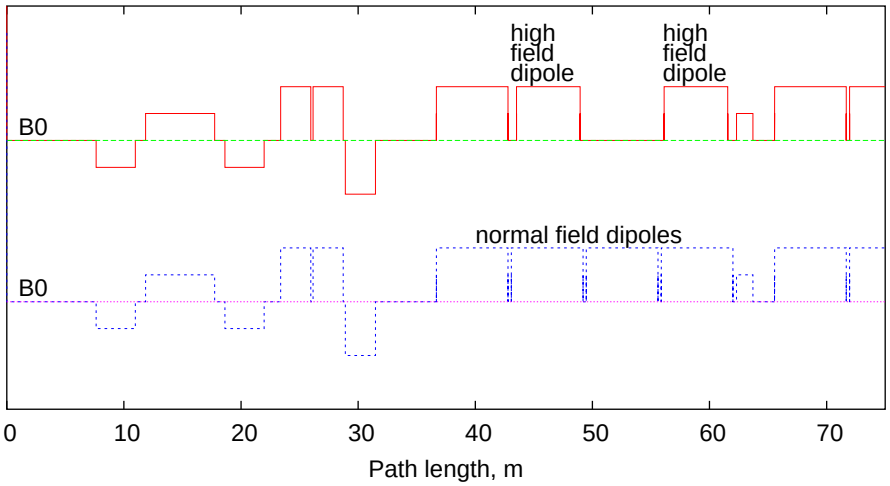

Figure 1: Tevatron Run-II lattice and lattice with two increased strength magnets instead of three normal strength magnets in the Tevatron B11 section. Magnetic field in two magnets is increased to 6.7 T compared to the normal field of 4.4235 T.

3 Detector Acceptance Modeling

The detector acceptance simulations are done via tracking of particles ejected from the IP with different momentum and angles. Initial particles distribution in the IP is shown in Fig. 5. For these calculations we took uniform distribution on momentum in the range of $0.7 < P/P_0 < 1$ and on p_t in the range of $0 < p_t < 5.7$ GeV/c. Results for the quadrupole and dipole Roman Pots acceptance are presented in this section both for proton and antiproton directions. Two-dimensional distributions show a number of events per bin, $\Delta p_t^2 = 0.1$ (GeV/c)$^2 \times \Delta p/p_0 = 0.006$, per the number of flat events generated at IP (10^6) per bin. Three cases have been studied:

1. Realistic Roman Pots with all interaction processes in their materials. Results for all 8 pots are superpositioned and shown in Fig. 6.

2. All Roman Pots are supposed to be a black hole. Results for all 8 pots are superpositioned and shown in Fig. 7.

3. All Roman Pots are supposed to be fully transparent. Results for all 8 pots are superpositioned and shown in Fig. 8. Results for all pots individually are shown in Fig. 9.

name	L	β_x	β_y	$10\sigma_x$	half-separation	$10\sigma_y$	half-separation	detector position	
	m	m	m	mm	horizontal, mm	mm	vertical, mm	hor., mm	ver., mm
CDFpq1	22.794	336	1086	10.20	0.130	18.35	0.235	$10\sigma_x$	$10\sigma_y$
CDFpq2	22.916	334	1081	10.18	0.130	18.31	0.235	$10\sigma_x$	$10\sigma_y$
CDFpq3	23.038	332	1077	10.15	0.130	18.28	0.235	$10\sigma_x$	$10\sigma_y$
CDFps1	31.882	209	772	8.04	0.018	15.47	0.218	$10\sigma_x$	$10\sigma_y$
CDFps2	32.004	207	768	8.02	0.018	15.43	0.218	$10\sigma_x$	$10\sigma_y$
CDFps3	32.126	205	764	7.99	0.018	15.40	0.218	$10\sigma_x$	$10\sigma_y$
RPOT1p	50.438	45	298	3.72	0.450	9.62	0.333	$10\sigma_x$	$10\sigma_y$
RPOT2p	52.540	34	259	3.25	0.499	8.96	0.347	$10\sigma_x$	$10\sigma_y$
RPOT3p	54.641	25	222	2.80	0.548	8.30	0.360	$10\sigma_x$	$10\sigma_y$
RPOT4p	162.147	54	60	4.10	2.118	4.32	0.854	$10\sigma_x$	$10\sigma_y$
RPOT5p	164.249	49	64	4.00	2.078	4.45	0.805	$10\sigma_x$	$10\sigma_y$
RPOT6p	166.350	45	68	3.74	2.037	4.60	0.757	$10\sigma_x$	$10\sigma_y$
RPOT6a	6118.383	72	49	4.72	0.812	3.92	1.868	$10\sigma_x$	$10\sigma_y$
RPOT5a	6120.485	67	54	4.57	0.855	4.10	1.921	$10\sigma_x$	$10\sigma_y$
RPOT4a	6122.586	63	60	4.42	0.898	4.30	1.975	$10\sigma_x$	$10\sigma_y$
RPOT3a	6224.503	162	13	7.08	0.380	2.03	0.580	$10\sigma_x$	$10\sigma_y$
RPOT2a	6225.516	177	16	7.41	0.374	2.23	0.565	$10\sigma_x$	$10\sigma_y$
RPOT1a	6226.528	193	19	7.73	0.368	2.43	0.551	$10\sigma_x$	$10\sigma_y$
CDFas3	6251.065	782	210	15.58	0.217	8.08	0.206	$10\sigma_x$	$10\sigma_y$
CDFas2	6251.187	786	212	15.60	0.216	8.10	0.205	$10\sigma_x$	$10\sigma_y$
CDFas1	6251.309	790	213	15.66	0.215	8.14	0.203	$10\sigma_x$	$10\sigma_y$
CDFaq3	6260.154	1102	339	18.50	0.235	10.25	0.131	$10\sigma_x$	$10\sigma_y$
CDFaq2	6260.276	1106	340	18.52	0.235	10.28	0.131	$10\sigma_x$	$10\sigma_y$
CDFaq1	6260.398	1111	342	18.56	0.236	10.31	0.132	$10\sigma_x$	$10\sigma_y$

Table 1: β -functions, $10\sigma_{x,y}$ size, orbit separation and detectors position with respect to the closed orbit.

The acceptance of the quadrupole spectrometers CDF is quite different from those of the dipole spectrometer RPOT. Because of the lack of a dipole field all particles with small p_t pass through the center and those with $p_t >$1 GeV/c are accepted almost independent of p/p_0. The dipole spectrometers (RPOT) allow to detect particles with very small p_t, and their momentum acceptance depends on the distance to the IP. Dipole spectrometers RPOT1-3 have broad momentum acceptance, but particles with $p/p_0 >$0.98 are not accepted. The dipole spectrometers RPOT4-6 located at large distance from the IP have small acceptance on momentum, but they accept particles with $p/p_0 >$0.98. The antiproton detector acceptance is similar to that of the proton ones both for quadrupole and dipole detectors. There are two small regions ($p_t <$0.5 GeV/c, 0.7$< p/p_0 <$0.84) and ($p_t <$0.7 GeV/c, 0.975$< p/p_0 <$0.985) which are not accepted by the Roman Pots. The system can be optimized to accept these particles by changing locations of the dipole Roman Pots. These particles can be accepted by Roman Pots located at the distance of 100-130 m from the BØIP.

4 Conclusions

The performed studies ensure a possibility of the forward spectrometer design which allows to accept all particles in the range of 0$< p_t <$2 GeV/c and 0.7$< p/p_0 <$1.

References

[1] I. S. Baishev, A. I. Drozhdin and N. V. Mokhov, "STRUCT Program User's Reference Manual", SSCL–MAN–0034 (1994); http://www-ap.fnal.gov/∼drozhdin/.

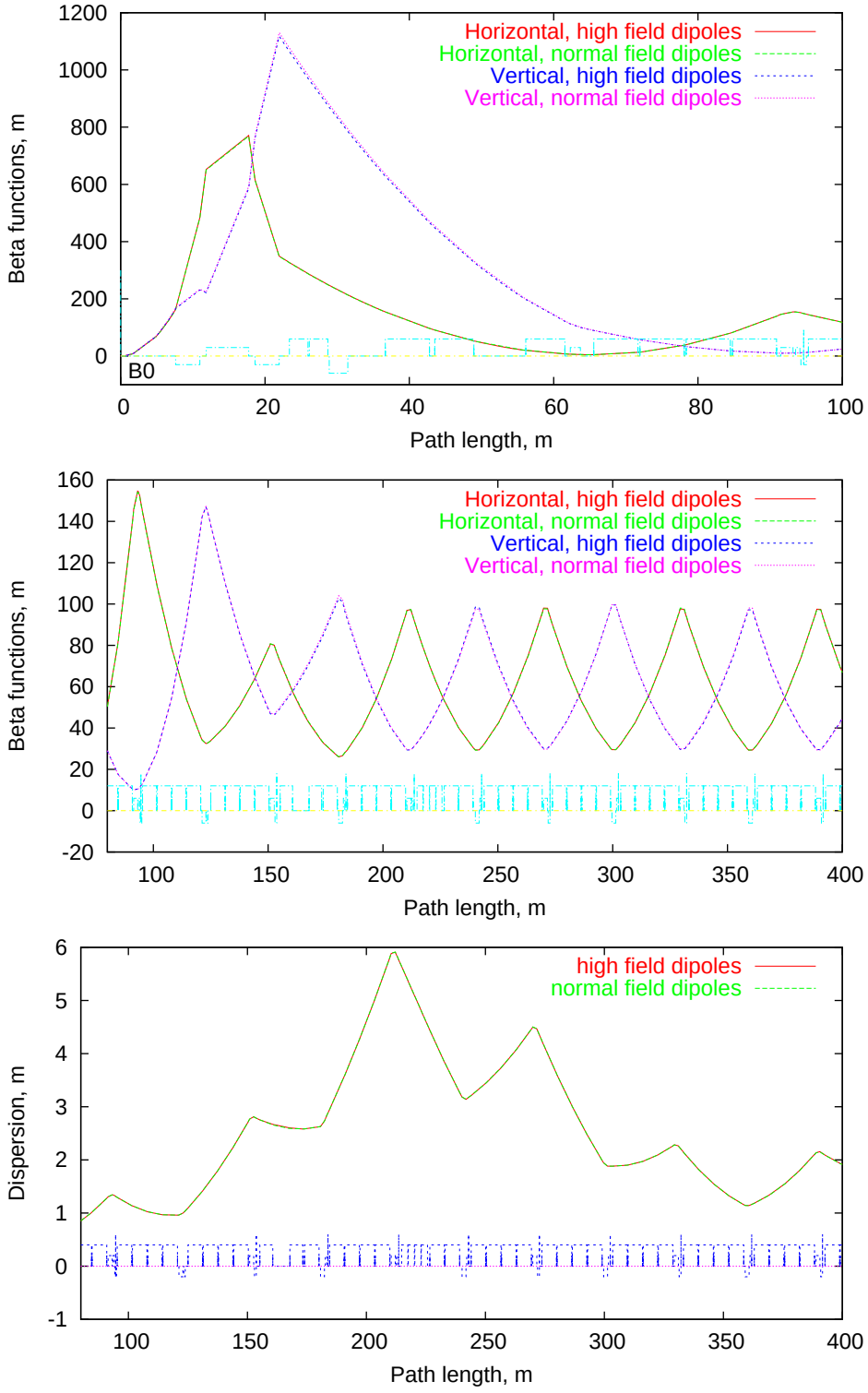

Figure 2: Horizontal and vertical β functions (top and middle) and horizontal dispersion (bottom) in the Tevatron Run-II lattice and lattice with increased strength of magnets in the Tevatron A44, B11 and B15 sections.

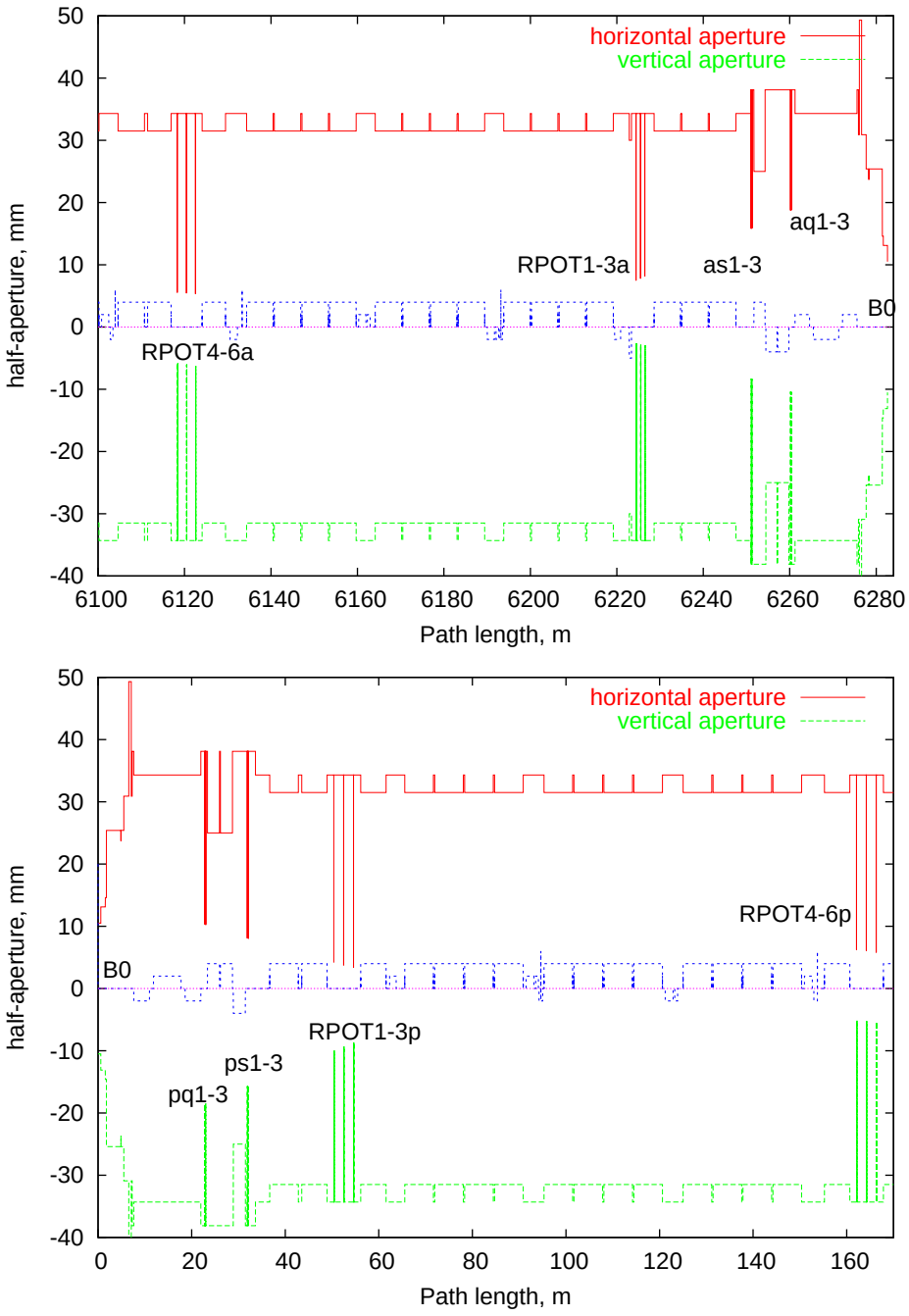

Figure 3: Aperture of accelerator upstream (top) and downstream (bottom) of BØ, and Roman Pots location.

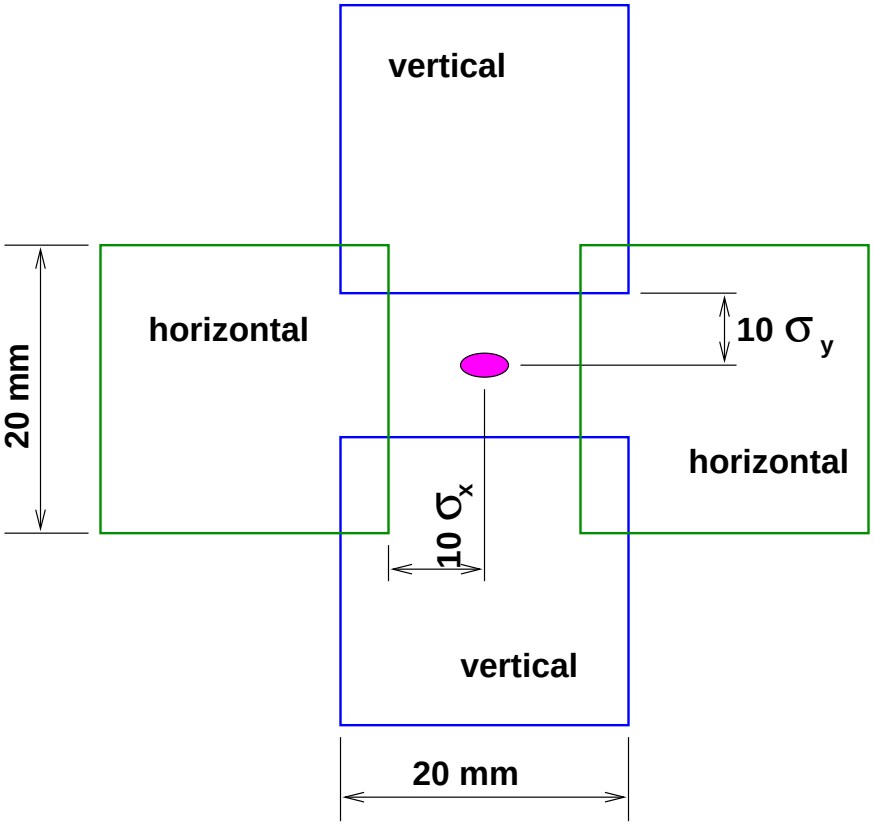

Figure 4: Roman Pots position with respect to the circulating beam.

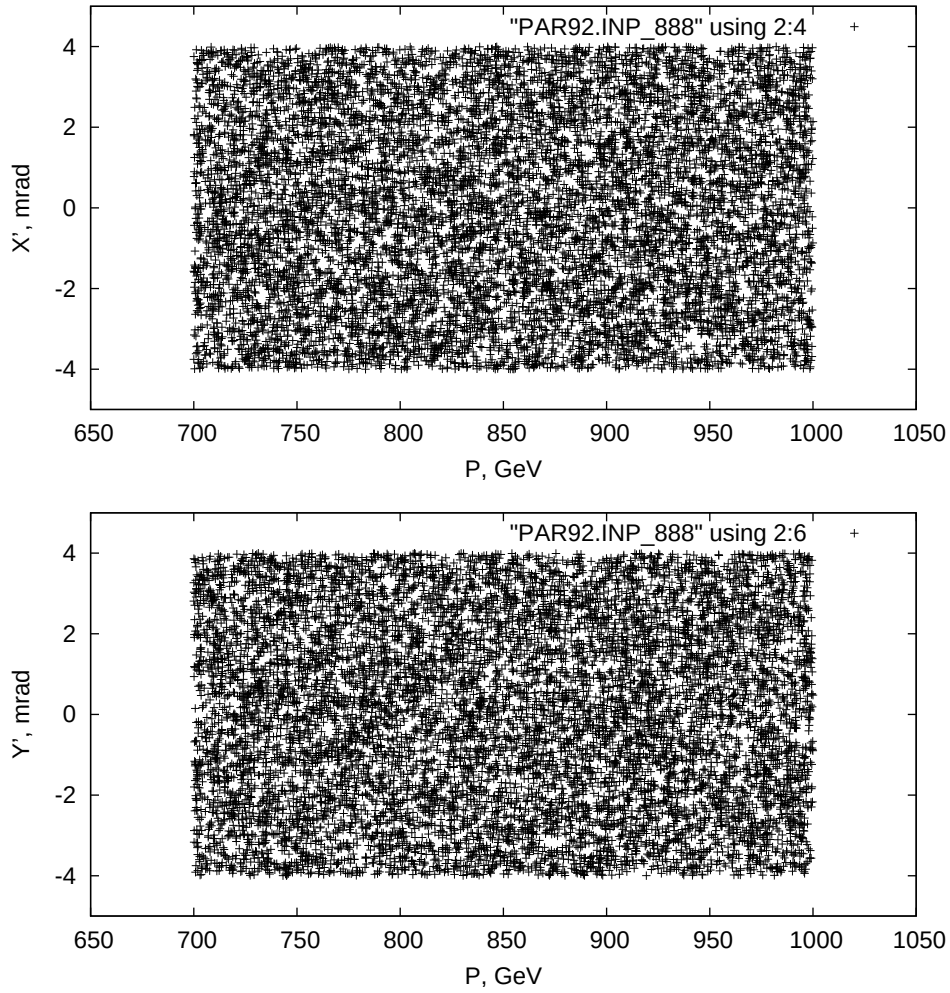

Figure 5: Initial particles distribution in the IP. (X=0.0, Y=0.0). 10^5 protons and 10^6 antiprotons are taken at the Roman Pots acceptance simulations.

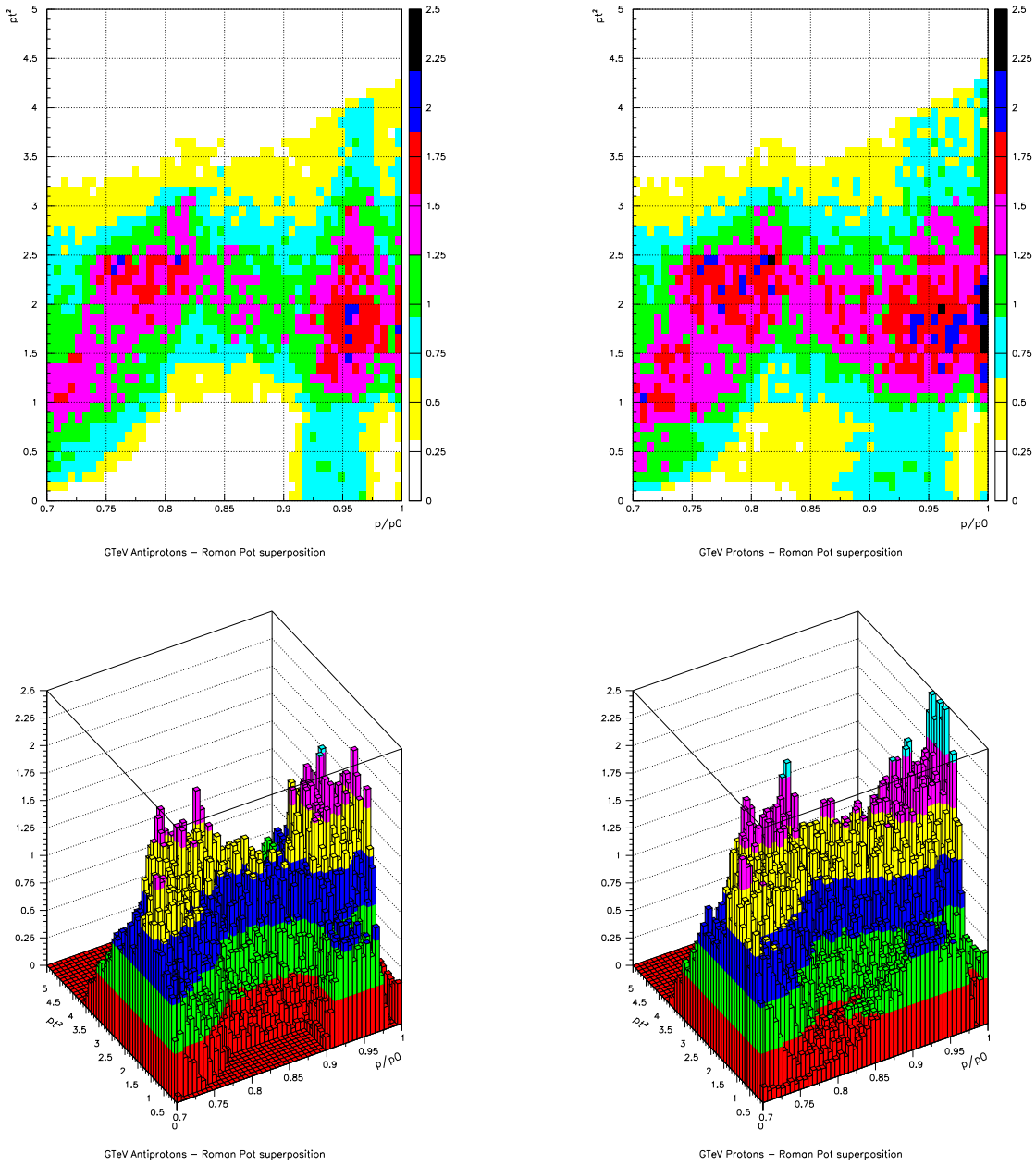

Figure 6: Roman Pot system acceptance for antiproton (left) and proton (right) directions for Case 1.

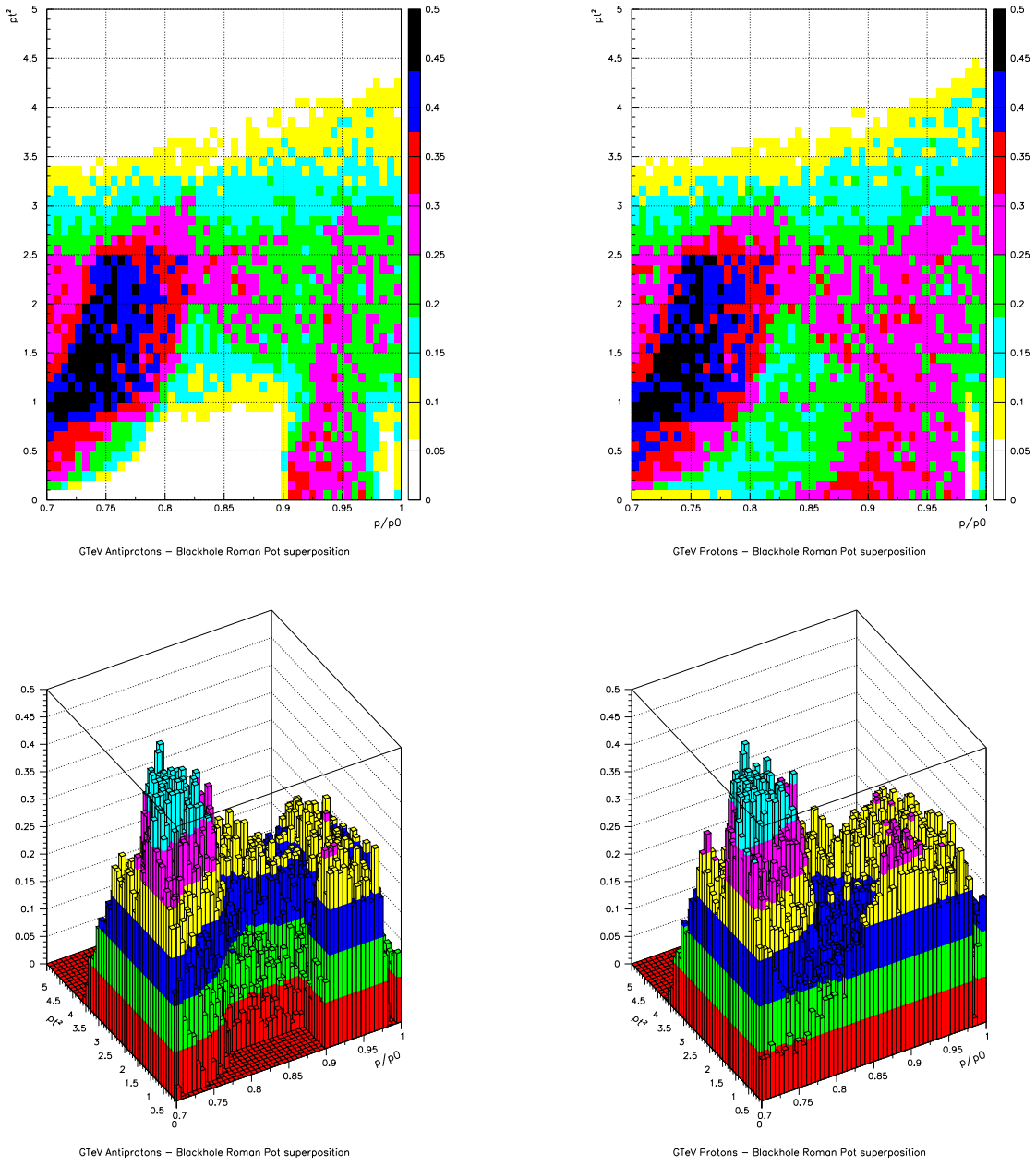

Figure 7: Roman Pot system acceptance for antiproton (left) and proton (right) directions for Case 2.

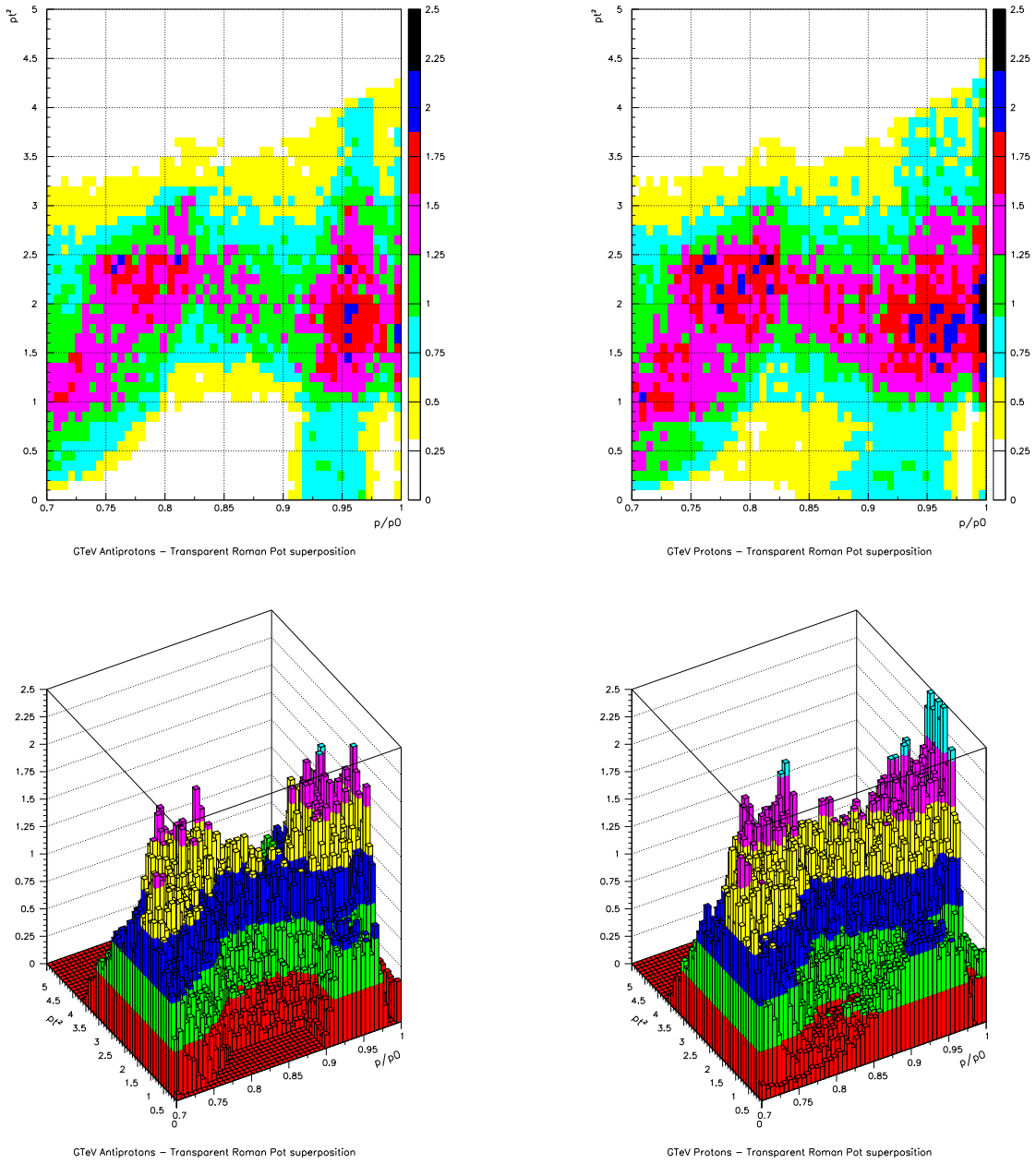

Figure 8: Roman Pot system acceptance for antiproton (left) and proton (right) directions for Case 3.

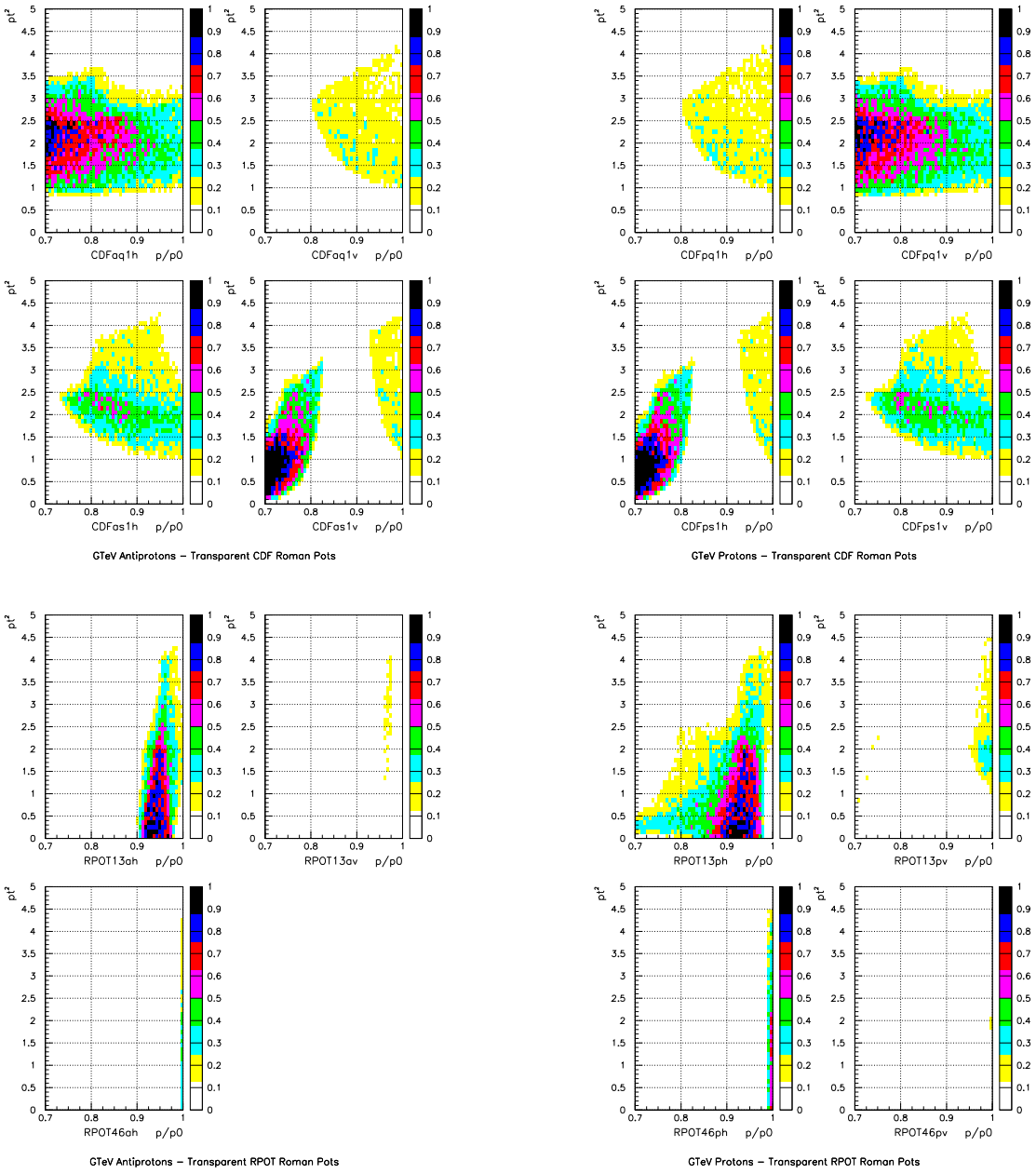

Figure 9: Acceptance of individual Roman Pots for antiproton (left) and proton (right) directions for Case 3.